Analytical Methods

Accepted Manuscript

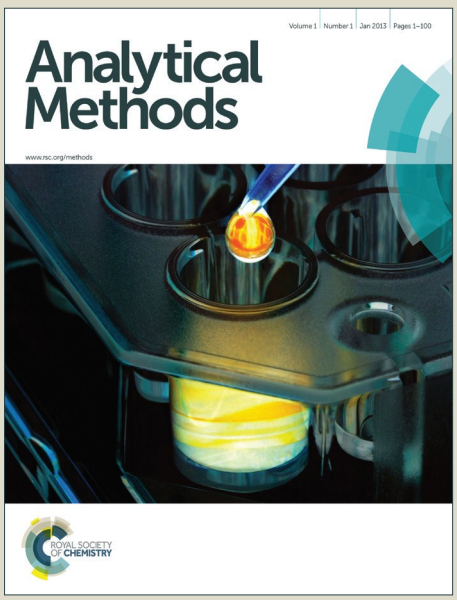

This is an *Accepted Manuscript*, which has been through the Royal Society of Chemistry peer review process and has been accepted for publication.

Accepted Manuscripts are published online shortly after acceptance, before technical editing, formatting and proof reading. Using this free service, authors can make their results available to the community, in citable form, before we publish the edited article. We will replace this *Accepted Manuscript* with the edited and formatted *Advance Article* as soon as it is available.

You can find more information about *Accepted Manuscripts* in the Information for Authors.

Please note that technical editing may introduce minor changes to the text and/or graphics, which may alter content. The journal's standard Terms & Conditions and the Ethical guidelines still apply. In no event shall the Royal Society of Chemistry be held responsible for any errors or omissions in this *Accepted Manuscript* or any consequences arising from the use of any information it contains.

ROYAL SOCIETY OF CHEMISTRY

www.rsc.org/methods

Cite this: DOI: 10.1039/c0xx00000x

www.rsc.org/xxxxxx

ARTICLE TYPE

Gold nanoparticles supported on zirconium, tin and ruthenium oxides for reagentless electrochemical sensing of hydrogen peroxide

Venkataraman Dharuman*, Chinnathambi Anjalidevi, Palinci Nagarajan Manikandan, Habibulla Imran

Received (in XXX, XXX) Xth XXXXXXXXX 20XX, Accepted Xth XXXXXXXXX 20XX

DOI: 10.1039/b000000x

Abstract

We demonstrated a simple method of metal oxide (M-Ox) supported gold nanoparticle (AuNP) composite film (M-Ox-AuNP) fabrication by mechanical and electrochemical methods on solid surface for reagentless electrochemical sensing of hydrogen peroxide (H_2O_2). The method involves anchoring the M-Ox onto the solid surface using nafion binder followed by electro deposition of AuNP to form M-Ox-AuNP composite. The M-Ox used are ruthenium (RuO_2), tin (SnO_2) and zirconium (ZrO_2) oxides. Studies reveal that the M-Ox-AuNP mimics the enzyme kineticbehaviour and Michaelis-Menten (MM) kinetic constants, K_M and K_C, are evaluated. The K_M values observed for the ZrO_2-AuNP, RuO_2-AuNP and SnO_2-AuNP composites are 1000, 10.1 and 2.3 mM, respectively. Highest K_M of the ZrO_2-AuNP is correlated with its largest band gap energy change (1.1 eV) and highest electrochemical activities. These are further supported by the increased crystalline nature and ligand-to-metal charge transfer processes confirmed by UV-visible spectroscopy (UV-Vis), Field Emission Scanning Electron Microscopy (FESEM), Fourier Transform Infrared (FTIR) and X-ray diffraction (XRD) techniques. These M-Ox-AuNP composites are applied for H_2O_2 sensing in commercial antiseptic and milk samples.

1. Introduction

Hydrogen peroxide (H_2O_2) is used regularly in disinfectant, textile bleaching and tooth cleaning processes. It is a by-product in many cellular reactions and its concentration dependence induces pulmonary disease. Hence, it's analytical determination is of most important in clinical, environmental and industrial applications. A number of techniques such as spectrophotometry[1], chemiluminescence[2,3] and electrochemistry[4,5] are reported to detect H_2O_2. Out of these, electrochemical method has advantages like fast response time, direct data correlation and easy miniaturization. To date, electrochemical sensors that use either horseradish peroxidase or hemoglobin along with metal oxides (zinc[2], iron[6], nickel[7], zirconium[8], tungsten[9] and silicon[10]) are reported for the direct H_2O_2 sensing. These metal oxides offer a biocompatible environment for the enzyme, enhance direct electron transfer rate (DET) and increase the stability and sensitivity.

Molecular Electronics Laboratory, Department of Bioelectronics and Biosensors, Science Block, Alagappa University, Karaikudi – 630 004 India.

**To whom correspondence should be addressed. V. Dharuman, E-mail: dharumanudhay@yahoo.com Phone: 91-4565-223361 Fax: 91-4565-225525*

Electronic Supplementary Information FTIR, UV, EIS, XRD, are available:. See DOI: 10.1039/b000000x

It is important to note that the preparation methods of these oxides and enzyme immobilization strategies are greatly influence the sensor performance[11-25]. Further, the enzymes are less stable and degraded easily by the environmental changes. Hence, avoiding the enzyme is advantageous in preparing robust sensor devices for long term applications. Recently, it has been shown that the metal oxide supported nanoparticles (gold and silver[26-34]) showed higher catalytic activities than their individual components. In this context, magnesium[35], titanium[27,36], cerium[37-41], aluminium[42,43], zirconium and ruthenium[44] oxides supported AuNP hybrid systems are reported for studying CO and H_2O_2 oxidation reactions. In most of these reports, both the oxide support and gold nanoparticle are prepared together and annealed to improve the crystalline nature, however, the catalytic effect of the AuNP is influenced by its structure and cagging effect by the respective metal oxide. In addition, sintering of the AuNP into crystals of different sizes and shapes influences the activity. Hence, coarsening of the AuNP with M-Ox needs to be avoided to improve the catalytic effect of the M-Ox-AuNP composites. Moreover, the catalytic efficiency of the M-Ox-AuNP composite depends on how hydrogen ion interacts with the AuNP[45] during the CO and H_2O_2 oxidation reactions. Although numerous metal oxides based H_2O_2 sensors are reported, till now, no report on comparing the catalytic activity of the AuNP supported on

different metal oxides for reagentless sensing of H_2O_2 by electrochemical method is reported in the literature, Scheme 1.

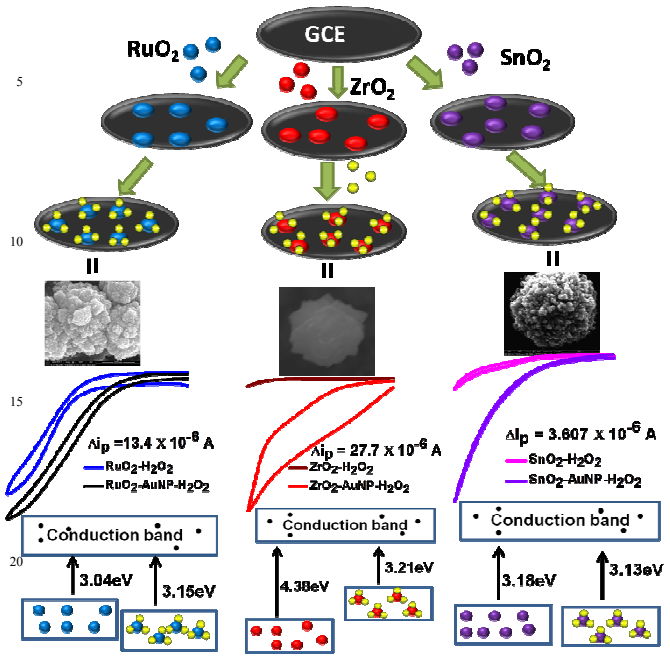

Scheme 1. Non-enzymatic H_2O_2 sensing at metal oxide-AuNP-nafion composites in phosphate buffer by electroreduction. Metal oxide-nafion is drop casted on the GCE and AuNP is electro deposited. Effect of AuNP on the detection sensitivity and the band gap energy obtained from optical spectra.

In this work, we prepared ZrO_2, SnO_2 and RuO_2 at a constant annealing temperature of 300 ºC. These oxides are anchored on an individual glassy carbon electrodes using nafion binder and then the M-Ox is decorated using AuNP by the electrolysis of $HAuCl_3.nH_2O$ at -0.2 V for 200 s. This method prevents the coarsening of the AuNP on the oxide surface and cagging effect by the metal oxide, which is commonly observed with the M-Ox-AuNP composites prepared by the thermal evaporation techniques. The reagentless H_2O_2 sensing by electrochemical studies reveals that the M-Ox-AuNP composites follow Michaelis-Menten (MM) kinetics. Hence, the effects of the AuNP on these oxide supports on the MM kinetic parameters, K_M and Kc are examined in detail by electrochemical techniques. Highest K_M and Kc values are noticed for the ZrO_2-AuNP than the other two composites. FESEM, UV-Vis, FTIR and XRD techniques are used to characterize these composites.

2. Experimental Section

2.1 Materials and Methods

Ruthenium (IV) Oxide, tin oxide, zirconium oxide, nafion (5%) and tetracholoroaurate were purchased from Sigma Aldrich, USA. Analytical grade NaOH, NaCl, KCl, Na_2HPO_4, NaH_2PO_4, catechol, uric acid, ascorbic acid and hydrogen peroxide were all purchased from Sisco Research Laboratories Chemicals Pvt. Ltd. India. Double distilled water was used for all experiments. A 0.01 M phosphate buffer containing NaCl (120 mm), NaH_2PO_4 (10 mM) and KCl (2.7 mM) was prepared and the pH was adjusted to 7.4 using NaOH and pH meter (Susima, AP-1PLVS, India). The CV, EIS and CA were carried out using CHI 604D electrochemical analyzer/workstation (CH Instruments, USA). A conventional three-electrode system consisting of glassy carbon working (3 mm diameter), platinum wire (1 mm diameter and 2 cm long) counter and Ag/AgCl reference electrodes was used. Bruker D8-Advanced powder diffractometer, which uses Cu-Kα1 radiation (2.2 kW max) was used for powder X-ray diffraction measurements (PANalytical B.V., Lelyweg 1, 7602 EA ALMELO, Netherland). Chemical vapor deposited gold (100 nm) coated Si substrates were used for acquiring the FESEM images and EDAX spectra using a Zeiss SEM instrument that uses LEO 1530 field emission (Hitachi model S-3000H, Japan). Images were recorded at an accelerating voltage of 10 kV with a secondary electron detector. FTIR spectra were recorded using the Perkin Elmer FTIR instrument. The UV-Vis spectra were measured using Schimadzu UV-Visible 2401 spectrophotometer.

2.2 Fabrication of zirconium, tin and ruthenium oxide supported gold nanoparticle composite films on GCE

Inactive hydrous oxides are converted into active catalysts by annealing them above 200 °C. Therefore, commercially procured RuO_2, ZrO_2 and SnO_2 were annealed at 300 °C for 1 hour in a muffle furnace and stored in a desiccator until use. Thus prepared oxides are used without any further pretreatments. 1% M-Ox (w/v) and 1% nafion (w/v) were mixed and sonicated for 15 minutes. 5 µL of the above mixture was drop casted on the GCE surface and air dried for 10 minutes. Following this, the AuNP was electro deposited from 0.2 mM $HAuCl_4.nH_2O$ by applying -0.2 V (Ag/AgCl) for 200 seconds. The results are highly reproducible and the error limit was within 10% of size variation. Prior to the electrochemical measurements, all solutions were degased with nitrogen for 10 minutes.

3. Results and Discussion

3.1. Characterization of ruthenium, zirconium and tin oxides supported gold nanoparticles and hydrogen peroxide sensing

Figure S1A shows the CVbehaviours of M-Ox-nafion (RuO_2, ZrO_2 and SnO_2) film modified GCEs before (curves a, c and e) and after electro deposition of AuNP (curves b, e and f), measured in phosphate buffer pH 7.4. The naïve oxides show no peak in the potential window studied (0 to -0.6 V (Ag/AgCl). The cathodic current (i_{pc}), measured at -350 mV, follows the order RuO_2 (5.1×10^{-6} A) > SnO_2 (1.96×10^{-6} A) > ZrO_2 (1.76×10^{-7} A), Fig.S1 (curves a, c and e). On the other hand, the M-Ox-AuNP composites exhibit wavelike peaks with increased charging current. The i_{pc} follows the same order (RuO_2-AuNP (7.30×10^{-6}A) > SnO_2-AuNP (4.86×10^{-6}A) > ZrO_2-AuNP (3.42×10^{-6}A)), however, differences exist in their individual voltammetricbehaviours, Fig.S1A. Similarbehaviours are noticed in NaOH and other electrolytes as well, Fig.S1B. This could be attributed to the nature of AuNP interaction with different M-Ox. Figure1 shows the comparative catalytic effects of the M-Ox and M-Ox-AuNP in the presence of 1 mM H_2O_2. The naïve ZrO_2 and SnO_2 poorly catalyze the H_2O_2 reduction, indicated by the

insignificant changes in their CV profiles (data not given for clarity). This could be related to their poor conducting nature of the ZrO_2 and SnO_2. In contrast, the naïve RuO_2 exhibits one order increased reduction current (from 6.88×10^{-6} to 6.00×10^{-5}A) in the presence of H_2O_2 due to its high conducting nature. Presence of AuNP on the RuO_2 and SnO_2 increases the H_2O_2 reduction current only by 1.2 times, while its presence on the ZrO_2 increases the reduction current by 10.2 times, Fig.1 and scheme 1. Figure S1C presents the effects of solution pH on the H_2O_2 reduction currents observed for the M-Ox-AuNP composites. The results reveal higher activity in the pH range 6-8 and maximum at pH 7.4. In order to understand these discrepancies, the UV-Vis and FESEM investigations are made further. The UV-Visbehaviours of the M-Ox-AuNP are depicted in Fig.S2. The presence of the AuNP on these metal oxide supports is signatured by an absorbance peak at 322 nm. This peak appears due to the charge transfer between the AuNP ligand and metal ion in the M-Ox-AuNP[46]. Along with this, another peak at 225-230 nm arise by the charge transfer from the surface oxide (O_2^-) ligand to the metal centre (M^{2+})[47,48] in the M-Ox-AuNP. Literally, it is reported that the co-prepared M-Ox-AuNP exhibit UV-Vis peak at 430 nm[47]. Hence, the blue shifted absorption peak at 335 nm (from 520 nm observed for pure AuNP) indicates hetero dispersed nature of the metal oxide and AuNP in the nafion matrix due to the sequential deposition. Band gap energies are calculated from the optical spectra using $(\alpha h\nu)^2$ versus $h\nu$ plots of the pristine M-Ox (RuO_2, ZrO_2 and SnO_2) and their respective M-Ox-AuNP composites, Fig. S2. The band gap energies of the M-Ox follow the order ZrO2(4.38 eV) > SnO_2 (3.18 eV) > RuO_2 (3.04 eV) [46-48] (Fig. S2). The band gap energies for the M-Ox-AuNP follow the order ZrO_2-AuNP (3.21 eV) > RuO_2-AuNP (3.15 eV) > SnO_2-AuNP (3.13 eV). The differences in the band gap energies are 0.09, 1.1 and 0.13 eV, respectively, for the RuO_2-AuNP, ZrO_2-AuNP and SnO_2-AuNP composites, Scheme 1. That is, the band gap energy difference is 10 times lowered for the ZrO_2-AuNP composite than the other two M-Ox-AuNP composites which showed an insignificant chang in the band gap. Hence, higher catalytic activity is observed with the ZrO_2-AuNP composite.

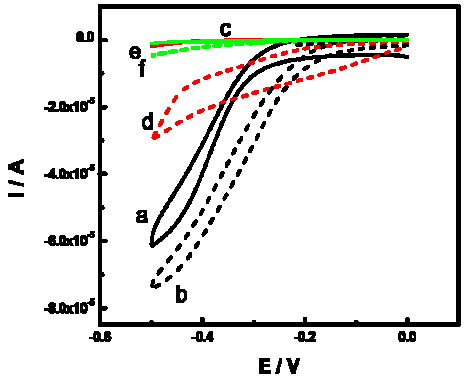

Fig. 1 CV behaviours of RuO_2-AuNP (curve a, b), ZrO_2-AuNP (curve c, d) and SnO_2-AuNP (curve e, f) modified GCEs in PBS measured at a scan rate 5 mVs^{-1} in the absence (curves, a, c, e) and presence (curves b, d, f) of 1 mM H_2O_2.

In order to probe the electrochemicalbehaviours of these M-Ox-AuNP composites further, the redoxbehaviours of the benchmark redox probes, $[Fe(CN)_6]^{3-/4-}$ and $[Ru(NH_3)_6]^{3+}$, are studied. The RuO_2 and RuO_2-AuNP showed insignificant redoxbehaviour (Fig.S3), whereas the ZrO_2 and ZrO_2-AuNP showed reversible and irreversiblebehaviours for both the redox probes, Fig.2.

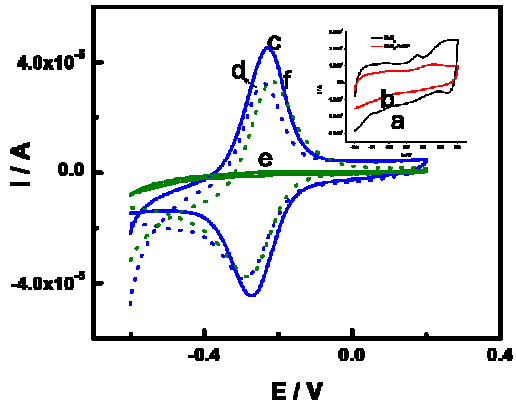

Fig. 2 CV behaviours of RuO_2-AuNP (curve a, b), ZrO_2-AuNP (curve c, d) and SnO_2-AuNP (curve e, f) modified GCEs in the absence (solid lines, curves, a, c, e,) and presence (dotted lines, curves b, d, f) of 0.1 mM $[Fe(CN)_6]^{3-/4-}$ in phosphate buffer measured at a scan rate 5 mVs^{-1}. Inset : enlarged view of RuO_2 and RuO_2-AuNP

Similarly, the SnO_2 and SnO_2-AuNP also exhibit reversible redoxbehaviours for both the redox probes, but the activity are lower than the ZrO_2-AuNP. This suggests that the activities of the oxide supported nobel metals occur via chemical sensitization influencing the surface potential, $eV_{surface}$, and the conductivity of the M-Ox-AuNP. The noble metals provide preferential active sites for the adsorption of target analyte. Similarly, presence of AuNP on the M-Ox surface changes the band gap energies. The smallest changes in the band gap energies of the RuO_2 and SnO_2 following the AuNP deposition are responsible for their low redox activities. This is further supported by the literature that the unusual behaviour of the ZrO_2-AuNP is observed in the water-gas shift reaction and is related to the presence of the AuNP clusters on ZrO_2 is highly active towards hydrogen atoms than the AuNP clusters present on the TiO_2 and CeO_2[45]. In those studies, the M-Ox-AuNP is prepared by the deposition - precipitation method and applied to study only gas phase catalytic reactions. However, in the present work, the M-Ox nanoparticles are pre-prepared by thermal decomposition method and the AuNP is sequentially deposited by the non-destructive electro reduction method. The heterogeneous reduction of H_2O_2 is made in phosphate buffer. In addition, the conductivity is dependent on the morphology of the sensing layer and bulk properties[49] of the M-Ox-NP composites.

The surface morphologies from FESEM measurements for all M-Ox and M-Ox-AuNP are presented in Fig.3. The pristine RuO_2 (Fig. 3, A) shows sponge like structure, whereas the ZrO_2 and SnO_2 (Fig. 3, B and C) show ball like crystalline structures. The presence of nafion in these oxides (Fig. 3, E) separates the particles from each other and prevents agglomeration (Fig. 3, D

and F). Better and distinct morphological changes are obtained for the AuNP deposited M-Ox surfaces. For example, the RuO_2-AuNP (Fig.3 G) exhibits cauliflower like structure, whereas the ZrO_2-AuNP (Fig.3 H) and SnO_2-AuNP (Fig.3 I) exhibit rose like a multilayered crystal cube (Fig.3 I) and ball like structures, respectively. These observations clearly suggest the differential interactions of the AuNP with these oxides, Scheme 1 and Fig.3.

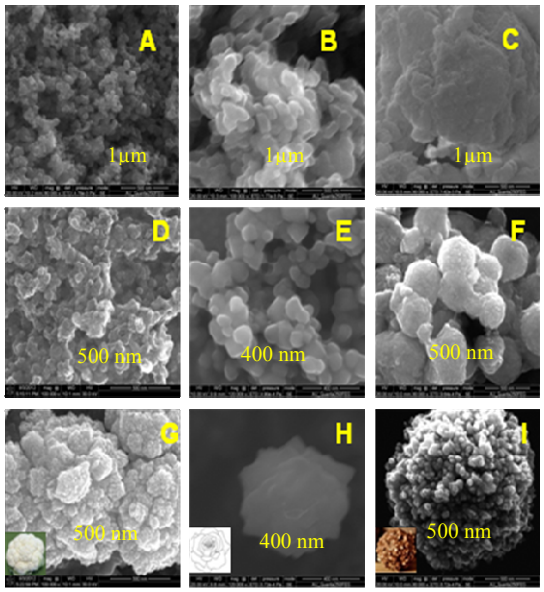

Fig. 3 SEM images of (A) RuO_2, (B) ZrO_2, (C) SnO_2, (D) nafion-RuO_2, (E) nafion-ZrO_2, (F) nafion-SnO_2, (G) RuO_2-AuNP, (H) ZrO_2-AuNP and (I) SnO_2-AuNP. Inset: natural cauliflower, rose and Rocher chocolate structures.

Figure 4 shows the XRD planes (110), (101), (111), (211) and (220) at 2θ 28, 34, 38.18, 54.3 and 65, respectively, for the RuO_2-AuNP (JCPDS # 880323 (RuO_2) and 652870 (Au)). This confirms rutail structure with the tetragonal geometry of the RuO_2[50]. The appearance of (111) and (220) planes indicate the synergistic interaction of AuNP with metal oxides[51,52]. But, the lone RuO_2 exhibit a single diffused and weak intense (110) plane due to its amorphous nature. Similar planes are obtained for the ZrO_2-AuNP and SnO_2-AuNP as well, however, with different intensities. The crystal size is calculated using Scherer formula $L = 0.9\,\lambda k\,\alpha/B_{2\theta}\,cos\theta_{max}$. Large change in the crystal size is noticed for the RuO_2 upon AuNP deposition and only small changes are observed for the ZrO_2 and SnO_2 following the AuNP deposition, Table S1. The deposition of AuNP enhances the size of RuO_2 crystal size by 5.7 times, ZrO_2 by 1.2 times and SnO_2 by 0.8 times. That is, the AuNP is more reactive on the RuO_2 than on the ZrO_2 and SnO_2.

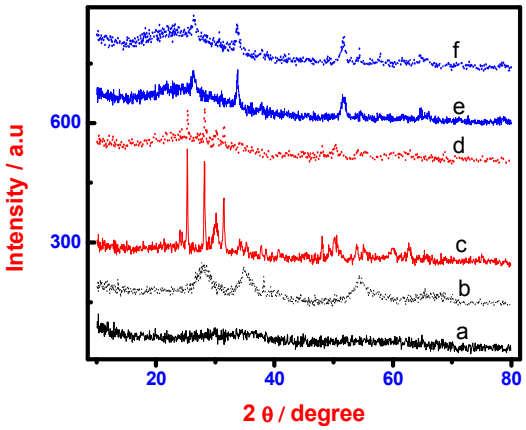

Fig. 4 XRD pattern of RuO_2 (curve a), RuO_2-AuNP (curve b), ZrO_2 (curve c), ZrO_2-AuNP (curve d) SnO_2 (curve e) and SnO_2-AuNP (curve f). Solid line: Pure metal oxides. Dotted line: metal oxide + AuNP in powder form.

The FTIR showed absorption bands at 600, 1050.2, 1130, 1400, 1575, 2230 and 3432 cm^{-1}, Fig. S4. The metallic character is indicated by the band in the frequency range 400 - 600 cm^{-1}. Presence of AuNP decreases the metallic character of ZrO_2, while it increases the same for the SnO_2 and RuO_2, as indicated by the increased band intensities in the frequency range 500 - 600 cm^{-1}, Fig. S4. Other than this, no significant changes are noticed (C-H (1391 cm^{-1}), C-C (1591 cm^{-1}) and O-H (~3300 cm^{-1}) stretching bands) for the ZrO_2-AuNP and SnO_2-AuNP compared to the RuO_2-AuNP. This could be related to the presence of large amounts of M-OH groups on the surface of the oxide supported AuNP. This hydration effect helps the M-Ox-AuNP to behave similar to the RuO_2 in solution phase, which mimics the peroxidase/catalase enzyme[53] behaviour.

Figure S5 shows the impedance behaviours of the M-Ox composites in phosphate buffer (pH 7.4) measured in the frequency range 100 kHz to 1 Hz at an applied DC potential -0.4 V. A straight line is observed at θ ~45° in the whole frequency range without semi-circle for both the RuO_2–AuNP and SnO_2-AuNP composites. The ZrO_2-AuNP composite showed partial semi circle behaviour. In other words, the charge transfer process is diffusion controlled at all M-Ox. The inset shows the equivalent circuit, $[R_s(Q_{CPE1}R1)(Q_{CPE2}R2)W)]$, used for mimicking the electrode/film interface and simulated data are indicated as circles. The circuit comprises solution resistance R_s, two constant phase elements (CPE, Q_{CPE}) representing the double layer capacitance and electrode roughness factor, two charge transfer resistances R_{CT} (R1 and R2) and a Warburg diffusion element, W. The series RQ may represent the inner M-Ox and outer M-Ox-AuNP catalytic layers of the nafion-M-Ox-AuNP composite. The CPE is defined by the equation $Z_{(\omega)} = 1/Q_{CPE}(j\omega)^n$. $\omega=2\pi f$ is the angular frequency and f is the frequency, n is the dimensionless CPE exponent indicating the degree of the surface roughness and in-homogeneity of the electrode surface that varies between 0.5 and 1. All composites show the lowest χ^2-value of $1.3 \pm 0.5\times10^{-4}$ confirming the accuracy of the simulated impedance data, Table S2. *R2* represents the R_{CT} of the M-Ox-

AuNP composite. Comparison of the charge transfer resistance suggests that the R_{CT} is increased for both the RuO_2-AuNP and SnO_2-AuNP and decreased for the ZrO_2-AuNP indicating the effective charge transport at ZrO_2-AuNP. The effect of H_2O_2 reduction on the R_{CT} is listed in Table S2.

3.2 Sensor Calibration

Effect of substrate concentration on the chrono amperometric behaviours of all the M-Ox-AuNP composites in the phosphate buffer is made. Shown in Fig. 5A is the comparative calibration curves obtained for the ZrO_2 and ZrO_2-AuNP. Current is measured after the *i-t* curve attains constant behaviour.

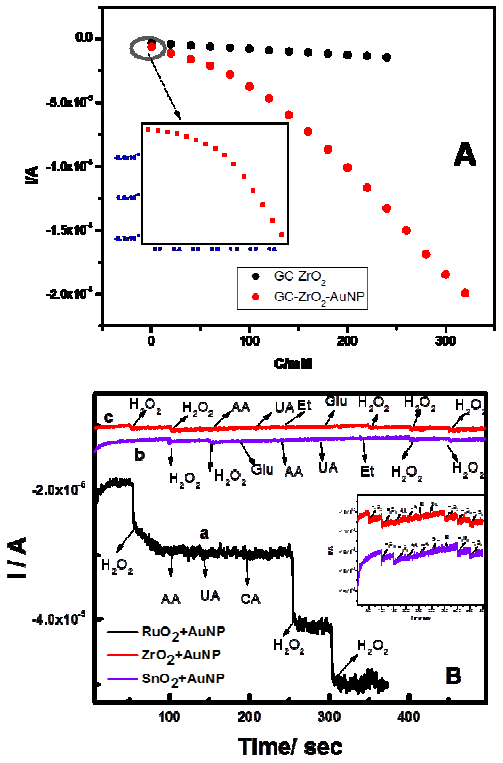

Fig. 5 (A) Comparative calibration curves obtained for ZrO_2 and ZrO_2-AuNP from chrono amperometry measurements made at -0.4 V for the successive addition of H_2O_2. Concentration range studied is 1×10^{-9} to 600×10^{-3} M. (B) CA response obtained for different M-Ox -AuNP for 1 mM H_2O_2 reduction at -0.4 V in presence of other potential interferences. UA: uric acid, CA: Catechol, AA: ascorbic acid, Et: Ethanol. Glu: glucose. Curve a: RuO_2-AuNP. Curve b: ZrO_2-AuNP. Curve c : SnO_2-AuNP

A saturation limit could not be observed for the ZrO_2-AuNP composite even after the addition of 500 mM H_2O_2 concentration. However, for the RuO_2-AuNP and SnO_2-AuNP composites the saturation limit is obtained in the concentration range, 0 - 30 mM, Fig5. The current *versus* concentration plots are given in Fig. S6 for all M-Ox-AuNP composites. Log (current) *versus* log (concentration) plot indicates the first order kinetics (slope = 0.98) at a lower substrate concentration range and zero order kinetics (slope =0.14) in the saturated concentration range, similar to that observed for the catechol oxidation[54] and glucose oxidation[50] on the RuO_2. That is, the reaction follows the pseudo first order kinetics in which the reaction rate is linear with the substrate concentration. The reaction between the H_2O_2 and M-Ox-AuNP following the Michaelis-Menten kinetics is represented by the following equation

$$\text{M-Ox}^{2+}\text{-AuNP} + H_2O_2 + 2e + 2H^+ \underset{K_c}{\overset{K_M}{\rightleftarrows}} [\text{M-Ox}^{2}\text{–AuNP-}\ H_2O_2] \rightarrow \text{M-Ox-AuNP} + H_2O + \tfrac{1}{2}\ H_2$$

The metal oxide forms an intermediate product. The MM kinetic equation for the reaction is written as $1/i = 1/nFAK_c\,\Gamma + K_M / nFAK_C\Gamma\, C_{H2O2}$ where K_M (moles lit^{-1}) and K_C ($cm\ s^{-1}$) are MM kinetic constants, n the number of electrons required for H_2O_2 reduction and it is 2 The Γ value for this purpose is calculated from the integration of the CV curve recorded at a low scan rate 5 mVs^{-1} in 1M NaOH, Fig. S1B and Table S3. The intercept and slope of LB plot, Fig. S7, are used to calculate the K_M and K_C values and summarized in Table S3. The K_M values obtained for the RuO_2-AuNP, ZrO_2-AuNP and SnO_2-AuNP composites are 10.1, 1000 and 2.3 mM, respectively. The K_M values indicate the maximum substrate concentration up to which the sensor signal varies linearly. Lower K_M values indicate higher affinity between the substrate and catalyst. Hence, the highest K_M of the ZrO_2-AuNP indicates its lower affinity for the H_2O_2 than the RuO_2-AuNP and SnO_2-AuNP composites. This is further supported from the lower diffusion rate of H_2O_2 at the ZrO_2-AuNP (D_r: 4.12 $\times$ 10^{-9} $cm\ s^{-1}$) than that observed for the RuO_2-AuNP (D_r 2.52 $\times$ 10^{-7} $cm\ s^{-1}$) and SnO_2-AuNP (D_r: 6.08 $\times$ 10^{-9} $cm\ s^{-1}$). The K_C values, defined as the turnover number are in the order 10^3 to 10^8 s^{-1}. This suggests that the reaction rate is similar to the enzymes carbonic anhydrase (10^5 s^{-1}), fumarase (10^2 s^{-1}) and ribonuclease (10^2 s^{-1}). This turn over number is several orders higher than that observed for the glucose oxidation at the RuO_2 surface itself. The non-enzymatic H_2O_2 catalysis using aqueous dispersed RuO_2 nanoparticles showed larger K_M (400 mM) due to larger quantity (5 mg mL^{-1}) of particles used and direct interaction of H_2O_2 at Ru metal center[54]. Hence, the lower K_M (10.1 mM) values noticed for the RuO_2-AuNP composite is related to the smaller amount of Ru metals available for H_2O_2 reaction when the same reaction was carried out heterogeneously on the electro surface. The different K_M values suggest clearly the role of metal oxide on the catalytic activities of AuNP in H_2O_2 detection. The wide linear range of 1 nm to 1000 mM observed for the ZrO_2-AuNP is not reported till now in the literature. Table S4 compares the H_2O_2 detections at different metal oxide and nanoparticle modified electrodes. It is to note that only our sensors showed the LOD in the range of nano molar range. The selectivity of these composite materials is studied next in presence potential interferences. All three composites showed high selectivity and specificity in the presence of potential interferences such as ascorbic acid, uric acid, catechol and dopamine in the PBS buffer, Fig. 5B. 1 mM of each of the interference is added sequentially in the same solution

at a regular interval of 50 s. In this work, external mediators and the enzyme HRP are avoided and, hence, direct detection of H_2O_2 is made. The M-Ox–AuNP composites are applied for the detection of H_2O_2 in antiseptic and commercial milk solutions. These real samples are used without further purification and pretreatments. All the M-Ox-AuNP composites detected the H_2O_2 in antiseptic solution. Different concentrations of the H_2O_2 in two different commercial milk samples (from indigenous vendors) are very well discriminated using the SnO_2-AuNP composite, Fig. S7, by their CV signal difference and the system is recovered with a RSD value of ± 3% for repetition of 4 times.

4. Conclusions

In summary, electro reduction of H_2O_2 is enhanced by the AuNP supported on the RuO_2, SnO_2 and ZrO_2 oxides. The reduction rate increases with increase in M-Ox crystalline nature and charge transfer between ligand-to-metal in the presence of the AuNP, confirmed by the of XRD, FTIR and UV-Vis spectroscopic techniques. This is in contrast to the gaseous CO oxidation reaction for which highest rate is observed on the amorphous M-Ox-AuNP surfaces. Comparison of three different oxide supports of different conducting nature suggests that the *ex situ* deposition of AuNP converts the inactive ZrO_2 into active oxide support. This is further supported by the similar quantity of the active metallic center observed for both ZrO_2 and SnO_2. The distinct morphologies of AuNP on these three M-Ox is reasonably correlated with the observed K_M values. The rose like structure of the AuNP on the ZrO_2 offers more active site and limited diffusion for the H_2O_2 reaction intermediates, enhances the K_M and lowers the affinity towards H_2O_2 for the ZrO_2-AuNP. While all M-Ox–AuNP composites detected the H_2O_2 concentrations in antiseptic solution, only the SnO_2-AuNP is able to detect the H_2O_2 in the commercial milk samples. This requires further basic research to improve the performance of the ZrO_2-AuNP for the analysis of other biological samples. Still, the method of M-Ox-AuNP preparation is very simple and can be easily adopted to design other metal oxide-gold nanoparticle systems and easily applied for other biomolecular sensing. Since nano structure influences greatly the interaction of target analytes, further work is in progress to develop M-Ox-AuNP composites with higher conductivity and diffusion restriction property using other polymers, tuning the metal oxide crystal sizes by methods like microwave irradiation and AuNP deposition conditions.

Acknowledgements

Dr. V. Dharuman acknowledges financial support from the Indian Council of Medical Research, New Delhi through the project (5/3/8/105/2013-RHN). The authors acknowledge Department of Industrial Chemistry, School of Chemistry, Alagappa University, Karaikudi, for providing FESEM and UV-visible spectroscopic facilities. P. N. Manikandan acknowledges the Department of Science and Technology(DST) for the award of INSPIRE Fellow (IF140744)

References

1 K. Sunil and B. Narayana, *Environ. Contam, Tox.* 2008, **81,** 422.
2 X. Lu, H. Zhang, Y. Ni, and Q. Zhang, J. Chen, *Biosens.Bioelectron,* 2008, **24,** 93.
3 W.W. Chen, B.X. Li, C.L. Xu, and L. Wang, *Biosens. Bioelectron,* 2009, **24,** 2534.
4 K.J. Huang, J.Y. Sun, C.X. Jin, Q.S. Jing, and T. Zhou, *Thin Solid Films,* 2011, **519**, 3925.
5 L.H. Zhang, Y.M. Zhai, N. Gao, D. Wen, and S.J. Dong, *Electrochem. Commun,* 2008, **10**, 1524.
6 G. Zhao, J.J. Xu, and H.Y. Chen, *Electrochem. commun.* 2006, **8**, 148.
7 A. Salimi, E. Sharifi, A. Noorbakhask, and S. Soltanian, *Electrochem. Commun,* 2006, **8**, 1499.
8 G. Zhao, J.J. Feng, J.J. Xu, and H.Y. Chen, *Electrochem. Commun,* 2005**, 7,** 724.
9 J.J. Feng, J.J. Xu, and H.Y. Chen, *Electrochem. Commun,* 2005, **8,** 77.
10 Y. Wang, X. Chen, and J.J. Zhu, *Electrochem. Commun,* 2009, **11,** 323.
11 J. Xuan, X. Jia, Li-P. Jiang, E.S. Abdel-Halim, and J.J. Zhu, *Bioelectrochemistry,* 2012, **84,** 32.
12 Y. Lin, X. Cui, and L. Li, *Electrochem. Commun*, 2005**, 7,** 166.
13 A. Salami, R. Hallaj, S. Soltanian, and H. Mamkhezria, *Anal. Chim. Acta,* 2007, **594**, 24.
14 Y. Ye, T. Kong, X. Yu, Y. Wu, K. Zhang, and X. Wang, *Talanta,* 2012, **89,** 417.
15 A.J. Wang, P.P. Zhang, Y.F. Li, J.J. Feng, W.J. Dong, and X.Y. Liu, *Microchim. Acta,* 2011, **175**, 31.
16 B. Xu, M.L. Ye, Y.X. Yu, and W.D. Zhang, *Anal. Chim. Acta,* 2010, **674,** 20.
17 J.J. Xu, Y.H. Bai, Y. Du, and H.Y. Chen, *Electrochem. Commun*, 2007, **9,** 255.
18 S. Palanisamy, S.M. Chen, and R. Saraswathi, Sens. *Actu. B* Chem*,* 2012, **167,** 372.
19 T.R.L.C. Paixao, M. Bertotti, *Electroanalysis,* 2008, **20,** 1671.
20 Q.Wang, and J. Zheng, *Microchim. Acta,* 2010, **169,** 361.
21 J. Ping, S. Ru, K. Fan, J. Wu, and Y.Ying, *Microchim. Acta,* 2010, **171**, 117.
22 S.J. Ling, R. Yuan, Y.Q. Chai, and T.T. Zhang, *Biopros. Biosyst. Eng,* 2009, **32,** 407.
23 J. Li, R. Yuan, Y. Chai, T. Zhang, and X. Che, *Microchim. Acta,* 2010, **171,** 125.
24 Y. Li, J. Zhang, H. Zhu, F. Yang, and X. Yang, *Electrochim. Acta,* 2010, **55,** 5123.
25 H. Zhong, R. Yuan, Choi, Yu. Zhang, C. Wang, and F. Jia, *Microchim. Acta,* 2012, **176**, 389.
26 S. Manivannan, and R. Ramaraj, *J.Chem Scienc,* 2009, **121,** 735.
27 S. Thiagarajan, B.W.Su, and S.M. Chen, Sens. *Actu. B* Chem*,* 2009, **136**, 464.
28 Y. Lee, M.A. Garcia, N.A. Frey Huls, and S. Sun, *Angew. Chem. Int. Ed,* 2010, **122**, 1293.
29 X. Huang, C. Guo, J. Zuo, N. Zheng, and G.D. Stucky, *Small,* 2009, **5**, 361.
30 A. Mills, and J. Reglinski, *Chem. Commun,* 2010, **46,** 2397.
31 C. A. Mirkin, R. L. Letsinger, R. C. Mucic, and J. J. Storhoff, *Nature,* 1996, **382**, 607.

32 S. Park, S. Oha, G. Ji-Young Mun, and S. Sik Han, *Colloid. Surf. B,* 2006, **48**,112.

33 T. A. Taton, C. A. Mirkin, and R. L. Letsinger, *Science,* 2000, **289**, 1757.

34 R. Meyer, C. Lemire, Sh.K. Shaikhutdinov, and H.-J. Freund, *Gold Bull,* 2004, **37**, 72.

35 Z. Yan, S. Chinta, A.A. Jr. J.P. Mohamed, Fackler, and D.W. Goodman, *J. Am. Chem. Soc,* 2005, **127,** 1604.

36 M.S. Chen, and D.W. Goodman, *Science,* 2004, **306**, 252**.**

37 V.A. Guerrero, and B.C. Gates, *J.Catal,* 2008, **260,** 351.

38 S. Carrettin, P. Concepción, A. Corma, J.M. Lopez Nieto, and V.F. Puntes, *Angew. Chem. Int. Ed,* 2004, **43,** 2538.

39 J. Guzman, S. Carretin, and A. Corma, *J. Am. Chem. Soc,* 2005, **127,** 3286.

40 J. Guzman, S. Carretin, J.C. Fierro-Gonzalez, Y. Hao, B.C. Gates, and A. Corma, *Angew. Chem. Int. Ed,* 2005, **44,** 4778.

41 J.A. Rodrigueza, X. Wanga, P. Liua, W. Wena, J.C. Hansona, J. Hrbeka, M. Perezb, and J. Evans, *Top Catal,* 2007, **44,** 73.

42 J. Wang, A.H. Lu, M. Li, W. Zhang, Y.S. Chen, D.X. Tian, and W.C. Li, *ACS Nano,* 2013, **7,** 4902.

43 A.F. An, A.H. Lu, Q. Sun, J. Wang, and W.C. Li, *Gold Bull,* 2011, **44,** 217.

44 L.F. Mattheiss, *Phys. Rev. B*, 1976, **13,** 2433.

45 M. Manzoli, A. Chiorino, F. Vindigni, and F. Boccuzzi, *Catalysis Today*, 2012, **181,** 62.

46 J.A. Peck, C. Drew Tait, B.I. Swanson, and G.E. Brown Jr, *Cosmochim. Acta,* 1991, **55,** 671.

47 S. Ivanova, C. Petit, and V. Pitchon, *Applied Catalysis A: General* 2004, **267,** 191.

48 M. Kitano, M. Matsuoka, M. Ueshima , and M. Anpo, *Applied Catalysis A: General,* 2007, **325,** 1.

49 M. E. Franke, T. J. Koplin, and U. Simon, *Small*, 2006, **2**, 36.

50 N. Bmrsan, and U. Weimar, *J. Electroceram,* 2001, **7**, 143.

51 V. Dharuman, and K.C. Pillai, *J. Solid State Chem,* 2006, **10,** 967.

52 A. Adeyemo, G. Hunter, and P.K. Dutta, Sens *Actuators B* Chem, 2011, **152,** 307.

53 P. Periasamy, S.W. Ting, and S.M. Chen, *Int. J. Electrochem. Sci,* 2011, **6,** 2688.

54 H. Deng, W. Shen, Y. Peng, X. Chen, G. Yi, and Z. Gao, *Chem. Eur. J.* 2012, **18,** 8906.

55 M.E.G. Lyons, C.H. Lyons, A. Michas, and P.N. Barlett, *Analyst*, 1992, **117,** 1271.